Journal of Science and Technology – Engineering and Technology for Sustainable Development
Volume 36, Issue x, Month 2026, 000-000

Fabrication and Characterization of Poly(lactic acid)/Chitosan Biocomposite Films for Controlled Oral Delivery of Lovastatin

Vu Quoc Manh[1], Dinh Ngoc Thao[2], Le Tien Dat[2], Nguyen Dang Dat[2], Vu Thi Huong[2], Nguyen Thi Bich Viet[2], Nguyen Ngoc Linh[1], Nguyen Thi Hong Nhung[1], Vu Quoc Trung[2,*]
[1]Institute of Medicine and Pharmacy, Thanh Do University, Ha Noi, Vietnam
[2]Faculty of Chemistry, Hanoi National University of Education, Ha Noi, Vietnam
[*]Corresponding author email: trungvq@hnue.edu.vn

Abstract

*Lovastatin **(Lov**), a lipid-lowering statin, suffers from low oral bioavailability due to poor solubility and extensive first-pass metabolism. The study developed poly(lactic acid)/chitosan (**PLA/Cs**) composite films incorporating **Lov** (5 – 20 wt.%) and examined how drug loading influences structural characteristics and release behavior. Films were prepared via a solution-based method. FT-IR analysis confirmed hydrogen bonding and dipole interactions among **PLA, Cs**, and **Lov**, while FESEM imaging revealed a morphological shift of **Lov** from rod-like crystals to spherical particles, with the **PLA/Cs** ratio of 5/5 and Lov accounting for 10 wt.% the total polymer (**PCL5510**), sample displaying the most uniform dispersion. Drug release followed a biphasic pattern: an initial burst release from surface-adsorbed drug, followed by sustained release governed by diffusion and polymer matrix degradation. Lov content strongly influenced release kinetics, with **PCL5510** achieving slow, stable release at pH 2.0 and accelerated release at pH 7.4, conditions favorable for intestinal absorption. These findings identify **PCL5510** as an optimal formulation for controlled oral delivery of statins and highlight the potential of **PLA/Cs**-based systems in drug delivery applications.*

Keywords: Biocomposites, chitosan, drug release, lovastatin, Poly(lactic acid).

1. Introduction

Cardiovascular diseases, particularly atherosclerosis and dyslipidemia, remain among the leading causes of mortality and disability worldwide. According to the World Health Organization (WHO), approximately 17.9 million people die each year from cardiovascular diseases, accounting for nearly 32% of all global deaths. Statins are the cornerstone of treatment, functioning as inhibitors of 3-hydroxy-3-methylglutaryl coenzyme A (HMG-CoA) reductase and thereby reducing endogenous cholesterol synthesis. Among them, lovastatin (Lov) is a well-established agent that effectively lowers lipid levels, improves endothelial function, reduces vascular inflammation, and prevents major cardiovascular events [1, 2].

Despite its therapeutic benefits, Lov faces significant pharmacokinetic challenges. Its very low water solubility (~1.3 µg/mL at 25 °C) leads to poor oral bioavailability (under 5%), necessitating higher doses that increase the risk of adverse effects, particularly hepatotoxicity and myopathy [3]. To address these limitations, numerous strategies have been developed to enhance Lov's solubility, bioavailability, and release kinetics, including nanoparticles, nanoemulsions, and biodegradable polymer-based systems [4, 5].

Poly(lactic acid) (**PLA**) is one of the most widely investigated biodegradable polymers due to its biocompatibility, established safety profile, and U.S. Food and Drug Administration (FDA) approval for various biomedical applications such as dissolvable sutures, vascular scaffolds, and controlled-release matrices [6]. **PLA** degrades into lactic acid, a natural metabolite, making it particularly attractive for pharmaceutical use. However, its inherent brittleness and limited control over drug release kinetics when used alone restrict its performance as a drug carrier. These shortcomings can be addressed by blending **PLA** with other biopolymers, with chitosan (**Cs**) being especially promising. Chitosan, a linear polysaccharide obtained from crustacean shells, contains abundant amino ($–NH_2$) and hydroxyl (–OH) groups, enabling hydrogen bonding and electrostatic interactions with drug molecules. Moreover, its bioadhesive and permeation-enhancing properties significantly improve the oral bioavailability of various active compounds [7, 8]. Therefore, the combination of **PLA** and **Cs** can yield a hybrid matrix with enhanced mechanical integrity, biocompatibility, and tunable drug release behavior.

Recent studies have investigated the incorporation of statins into biodegradable polymer systems to reduce systemic toxicity and maintain sustained plasma

p-ISSN 3093-3242
e-ISSN 3093-3579
https://doi.org/10.51316/jst.xxx.etsd.2026.36.x.x
Received: Oct 14, 2025; Revised: Nov 27, 2025
Accepted: Dec 15, 2025; Online: Jan 20, 2026.

concentrations. Lov-loaded polymer nanostructures, for example, have demonstrated improved absorption and prolonged release relative to crystalline drug forms [4]. However, most prior work has focused primarily on formulation design, with limited attention given to the effect of drug loading content on release kinetics, a critical factor for optimizing clinical performance.

In this context, the present study aims to fabricate and characterize **PLA/Cs** composite films loaded with varying amounts of Lov, and to systematically analyze how drug content influences release kinetics under simulated gastric (pH 2.0) and physiological (pH 7.4) conditions. This dual-material platform not only addresses the limitations of **PLA** and **Cs** when used individually but also offers a tunable system for optimizing controlled drug release. The findings are expected to provide new insights into the design of hybrid polymeric drug carriers for Lov and potentially other poorly water-soluble statins, thereby contributing to safer, more effective, and clinically adaptable strategies for cardiovascular disease management.

2. Materials and Methods

2.1. Chemicals

Chitosan (**Cs**) (≥ 95%, deacetylated), viscosity 100 – 200 mPa.s, from shrimp shells from Aladdin (China); Lovastatin (≥ 95%) (**Lov**) from Rhawn (China); Poly(Lactic) Acid (**PLA**), Mw: 65,000 g/mol, melting point 264 – 269 °C, supplied by Sigma-Aldrich (USA). Other chemicals such as acetic acid (AcOH), dichloromethane (DCM), ethanol (EtOH), potassium chloride, sodium hydroxide, potassium hydroxide, and monopotassium phosphate, supplied by Xilong (China), were used directly without further purification.

2.2. Fabrication of Lov-loaded PLA/Cs Composites

The **PLA/Cs/Lov** biocomposite samples were fabricated using the solution method as described in Fig. 1. The specific steps are as follows:

Step 1: PLA was disolved in dichloromethan (solution **A**). **Lov** was disolved in ethanol (solution **B**). **Cs** was disolved in a 1% CH_3COOH solution (solution **C**).

Step 2: Solution **B** was then slowly added to solution **A** using a burette while homogenizing at 20,000 rpm for 5 minutes. The resulting solution was continuously stirred on a magnetic stirrer at 400 rpm for 1.5 hours to obtain solution **T**.

Step 3: Solution **C** was slowly added to solution **T** using a burette at a rate of 3 mL/min while simultaneously homogenizing at 20,000 rpm. The mixture was then continuously stirred on a magnetic stirrer at 400 rpm for 1 hour.

Step 4: Finally, the mixture was homogenized for an additional 5 minutes at 20,000 rpm, then poured into a petri dish and allowed to evaporate naturally to obtain the **PLA/Cs/Lov** film.

The sample notations and the composition of the composite samples are presented in Table 1.

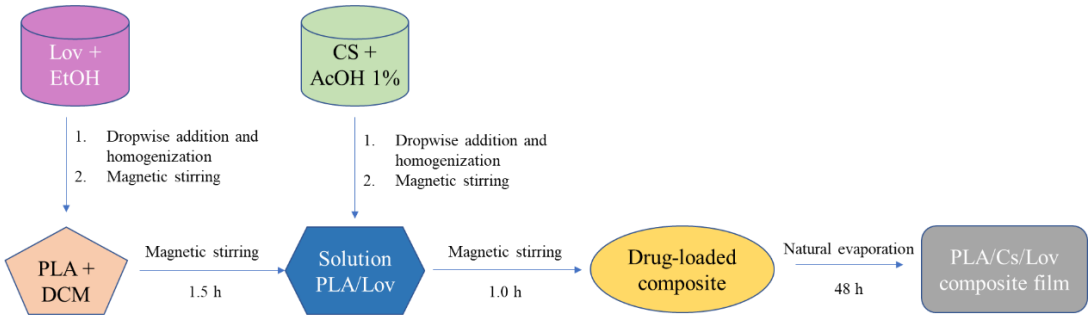

Fig. 1. Step-by-step scheme of **PLC/Cs/Lov** composite preparation

Table 1. Sample notations and compositions

No.	Sample notation	PLA (g)	Cs (g)	Lov (g)
1	**PCL555**	0.237	0.237	0.024
2	**PCL557**	0.242	0.242	0.034
3	**PCL5510**	0.250	0.250	0.05
4	**PCL5515**	0.232	0.232	0.0696
5	**PCL5520**	0.245	0.245	0.098

2.2. Characterization of PLA/Cs/Lov Composites

The following methods were used to characterize the PLA/Cs/Lov composites and evaluate drug release behavior:

Fourier Transform Infrared Spectroscopy (FT-IR): The infrared spectra of PLA/Cs/Lov biocomposite materials were recorded on a Nexus 670 FTIR spectrometer (USA).

Ultraviolet–Visible (UV–Vis) Spectroscopy: The concentration of Lovastatin in buffer solutions (pH 2.0 and pH 7.4) after release experiments was determined using a YOKE UV1900 Double Beam

Spectrophotometer (China). Samples were scanned in the range of 200 – 400 nm. Data were processed using Microsoft Excel to obtain calibration curves by linear regression.

Field Emission Scanning Electron Microscopy (FESEM): The morphology of the composite particles and the surface structure of **PLA/Cs/Lov** films were examined using a Hitachi S-4800 FESEM (Japan). Samples were coated with a thin platinum layer to prevent charging before imaging.

Differential Scanning Calorimetry (DSC): Thermal behavior of the composite samples was analyzed with a Shimadzu DSC-60 calorimeter (Japan). Measurements were conducted under a nitrogen atmosphere (10 mL/min), with heating from room temperature to 200 °C at 10 °C/min.

***In Vitro* Lov-release Studies:** Drug release experiments were performed on crystalline **Lov** and **PLA/Cs/Lov** composite films in simulated gastric fluid (pH 2.0) and simulated intestinal fluid (pH 7.4) at 37.0 ± 0.1 °C. Samples of predetermined mass were immersed in 200 mL of buffer solution and stirred at 200 rpm using a six-position dissolution tester (Guoming, China). At fixed time intervals (1 h), 5 mL aliquots were withdrawn and immediately replaced with fresh buffer to maintain a constant volume. The concentration of dissolved **Lov** was determined by UV–Vis absorbance at 238.8 nm using the calibration curves:

$$\text{pH 2.0: } A_{238,8nm} = 1325.7 \times C_{Lov,\,ppm} + 0.0599 \quad (1)$$

($R^2 = 0.9916$, $LOD = 3.24\times10^{-6}$ ppm, $LOQ = 9.81\times10^{-6}$ ppm).

$$\text{pH 7.4: } A_{239,6nm} = 21956 \times C_{Lov,\,ppm} + 0.0412 \quad (2)$$

($R^2 = 0.9951$, $LOD = 1.95\times10^{-7}$ ppm, $LOQ = 5.92\times10^{-7}$ ppm).

where:

A – the absorbance;

C – the concentration of Lov released at time t;

LOD – Limit of Detection;

LOQ – Limit of Quantitation.

All experiments were conducted in triplicate to ensure reproducibility.

The percentage of Lovastatin released from the composite samples in these solutions was calculated using the following formula:

$$H\,(\%) = \frac{m_t}{m_o} \times 100 \quad (3)$$

where:

H – the percentage of **Lov** released at the time of study (%);

m_t – mass of Lov released at the time of study;

m_o – initial mass of Lov in the composite sample.

3. Results and Discussion

3.1. FT-IR Spectra of PLA/Cs/Lov Composites

The FT-IR spectra of pure **PLA**, **Cs**, and **Lov** (Fig. 2) exhibit distinct absorption bands that reflect their characteristic functional groups. These spectra not only confirm the molecular structures of the individual components but also provide a foundation for evaluating potential intermolecular interactions in the composite system.

The spectrum of **PLA** is dominated by a sharp band at 1748 cm^{-1} corresponding to the ester carbonyl stretching vibration ($\nu_{C=O}$). Weak absorptions in the range of 2995 – 2845 cm^{-1} are attributed to Csp^3–H stretching, while a strong band at 1082 cm^{-1} is assigned to C–O stretching. A medium-intensity band at 1459 cm^{-1} arises from $–CH_3$ bending. Additionally, signals at 1655 cm^{-1} (amide I, from residual N-acetyl groups) and 1580 cm^{-1} ($\delta_{N–H}$ or $\nu_{C–N}$) suggest incomplete deacetylation during polymer processing [9]. The **Cs** spectrum exhibits a strong, broad band at 3362 cm^{-1}, representing overlapping O–H and primary amine N–H stretching vibrations. A weak absorption at 2911 cm^{-1} is assigned to –CH stretching, while a strong peak at 1029 cm^{-1} corresponds to C–O stretching. The $\delta_{N–H}$ bending vibration of the primary amine group appears at 1582 cm^{-1}, and intense signals in the 1070 – 1020 cm^{-1} region reflect C–O–C and C–O–H vibrations associated with the pyranose ring framework [10-12]. The spectrum of **Lov** shows a distinct –OH stretching band at 3537 cm^{-1}. Multiple peaks at 2964, 2928, and 2865 cm^{-1} correspond to Csp^3–H stretching. Two sharp, well-defined bands at 1722 and 1697 cm^{-1} confirm the presence of lactone carbonyl groups ($\nu_{C=O}$), while a strong absorption at 1067 cm^{-1} is attributed to C–O stretching [13, 14].

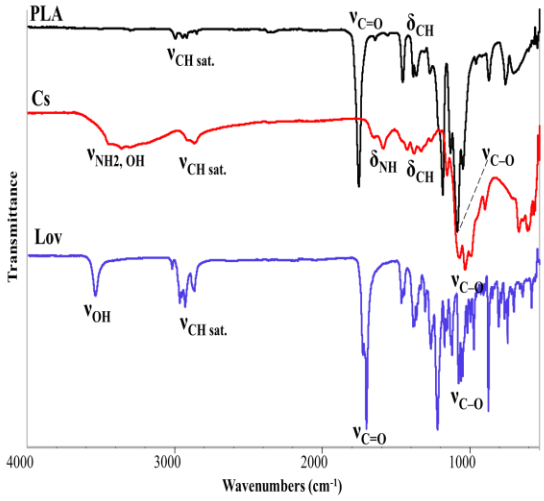

Fig. 2. FT-IR spectra of pure **PLA, Cs**, and **Lov**

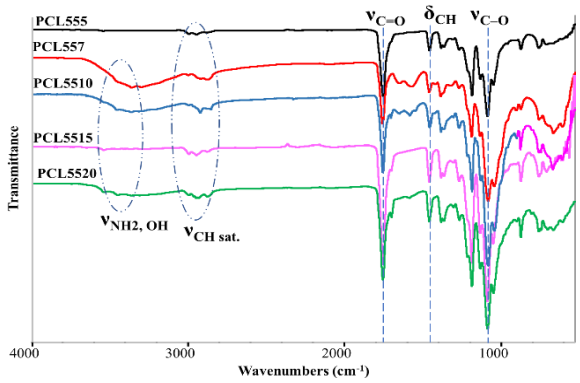

Fig. 3. FT-IR spectra of **PCL55x** composites with various **Lov** content (x)

The FT-IR spectra of the **PCL55x** composite samples exhibit all the characteristic absorption bands of **PLA**, **Cs**, and **Lov** (Fig. 3). Importantly, the appearance of these signals with slight shifts in frequency relative to the spectra of the individual components suggests the occurrence of intermolecular interactions within the composite system. For instance, the ester carbonyl stretching band (($\nu_{C=O}$)) in the spectrum of **PCL5510** is observed at 1750 cm^{-1}, representing a shift of approximately +2 cm^{-1} relative to **PLA** (1748 cm^{-1}) and +28 cm^{-1} compared to **Lov** (1722 cm^{-1}). Likewise, the broad band assigned to O–H and N–H stretching in **Cs** (3362 cm^{-1}) shifts downward by 174 cm^{-1} compared with the –OH band of **Lov** (3537 cm^{-1}), appearing at 3363 cm^{-1} in the composite spectrum.

These spectral shifts provide strong evidence for intermolecular hydrogen bonding between the –NH_2 and –OH groups of **Cs** and the carbonyl groups of **Lov**. Such interactions are known to stabilize drug–polymer matrices and influence both the morphology and release characteristics of the resulting composites [13, 15]. The observed changes are consistent with prior reports on polymer–drug carrier systems, where hydrogen bonding and electrostatic forces commonly lead to measurable variations in the position and intensity of carbonyl and hydroxyl vibration bands.

Taken together, the FT-IR data, as summarized in Table 2, confirm not only the successful incorporation of **Lov** into the **PLA/Cs** matrix but also the formation of stabilizing interactions that are likely to play a critical role in controlling drug release behavior.

3.2. Morphology of PCL55x Composites

FESEM observations provide important insights into the dispersion state and morphological characteristics of **Lov** within the **PLA/Cs** matrix (Fig. 4). Pure **Lov** is clearly visible in its crystalline form, appearing as flakes, lamellar structures, or irregular flat pieces with rough surfaces, reflecting its intrinsic crystalline nature [16, 17]. These crystals are relatively large, typically in the range of 5 – 10 µm. However, during composite preparation, **Lov** was pre-dissolved in ethanol, and upon incorporation into the polymer matrix, its morphology transformed into smaller, more spherical particles. The **PLA/Cs** blend forms a porous matrix framework with numerous voids, which facilitate the entrapment and dispersion of **Lov** within the material. Nevertheless, the particle distribution is non-uniform, and agglomeration occurs depending on both the polymer–drug interactions and the drug loading content.

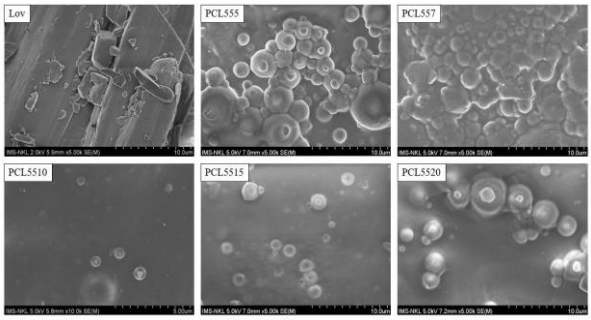

Fig. 4. FESEM images of pure **Lov** and **PCL55x** composites

Table 2. Characteristics wavenumbers of the functional groups for **PLC, Cs, Lov**, and **PCL55x** biocomposites

ν (cm^{-1})	**PLA**	**Cs**	**Lov**	**PCL555**	**PCL557**	**PCL5510**	**PCL5515**	**PCL5520**
ν_{OH}, ν_{NH2}	-	3362	3537	-	3359	3361	3538	3454
$\nu_{CH\ sat.}$	2995 2950 2913 2845	2911 2865	2964 2928 2865	2997 2944 2876	2999 2875	2918	2991 2945 2872	2993 2945 2869
$\nu_{C=O}$	1748	-	1722 1697	1749	1752	1750	1749	1751
δ_{NH}	-	1582	-	-	1566	1574	-	-
δ_{CH}	1459	1374	1384	1381	1381	1381	1381	1381
ν_{C-O}	1082	1029	1069	1083	1077	1078	1073	1082

We observed that the drug loading content plays a decisive role in determining particle morphology and uniformity. Specifically, samples at both low loadings (**PCL555, PCL557**) and high loadings (**PCL5515, PCL5520**) exhibit a tendency for non-uniform distribution, clustering, and agglomeration of Lov particles. This aggregation is visible as dense clustering in the lower-loaded samples (**PCL555, PCL557**). In contrast, the **PCL5510** formulation (10 wt.% Lov) achieved markedly improved dispersion, characterized by well-formed spherical particles with sizes in the range of 0.2 − 0.5 μm. This enhanced morphology can be attributed to stronger intermolecular interactions, including dipole–dipole interactions between protonated NH_3^+ groups in **Cs** (generated in the CH_3COOH environment) and hydrogen bonding between the –OH and $–NH_2$ groups of **Cs** with **Lov** [15]. These findings confirm that controlling the drug loading to the optimal point (**PCL5510**) is essential to prevent both insufficient molecular interaction (at low loads) and the partial recrystallization (at high loads) that leads to undesirable burst release effects.

The drug loading content plays a decisive role in determining particle morphology. At higher **Lov** contents, partial recrystallization or precipitation occurs, producing larger particles, sometimes with hollow or irregular structures. Such morphological features directly influence drug-release behavior: larger crystalline particles or particles with rough/porous surfaces are prone to an initial "burst release," while smaller, more uniform, spherical particles favor a gradual and sustained release profile [18, 19].

Overall, these findings highlight the importance of optimizing drug loading to balance dispersion quality and morphological stability, thereby achieving controlled-release characteristics desirable for pharmaceutical applications.

3.3. Thermal Properties of the PCL55x Composites

The results of DSC analyses obtained for pure **Lov** and **PCL55x** composite materials with varying **Lov** contents are presented in Fig. 5 and Table 3.

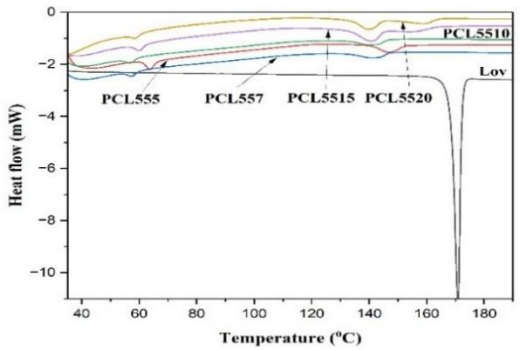

Fig. 5. DSC thermograms of pure **Lov** and **PCL55x** composites

Table 3. DSC results of **Lov** and **PCL55x** composites

Sample	1st endothermic peak (°C)	T_m (°C)	2nd endothermic peak (°C)
Lov	-	-	174.6
PCL555	63.9	145.7	-
PCL557	62.4	143.6	-
PCL5510	68.8	142.9	-
PCL5515	66.4	141.2	157.9
PCL5520	64.7	140.8	160.3

As shown in Fig. 5, a sharp endothermic peak is observed at 174.6 °C for pure **Lov**, corresponding to its melting point. The melting process begins at ~172 °C and ends at ~177 °C, which is consistent with previously reported data [20]. Whereas, in the **PLA/Cs/Lov** composites, notable differences emerge depending on drug loading. For the **PCL555**, **PCL557**, and **PCL5510** samples, the characteristic melting peak of **Lov** nearly disappears. This indicates that **Lov** is largely converted into an amorphous state or molecularly dispersed within the polymer matrix **PLA/Cs**. Previous studies indicated that the melting temperature (T_m) of Lov in the chitosan/alginate polymer matrix was reduced, yet remained higher than when incorporated into the **PLA/Cs** polymer matrix. Similar results were observed for lovastatin solid dispersions utilizing PVP K30 [21] or a combination of PEG 4000 and PVP K30 [22]. Thus, the **PLA/Cs** system demonstrates better Lov dispersion capability. Such amorphization is advantageous, as it significantly enhances the solubility and dissolution rate of **Lov**, which is otherwise limited by its poor aqueous solubility [23]. At higher drug loadings (**PCL5515** and **PCL5520**), a weak endothermic signal reappears in the melting region of **Lov**, although with much lower intensity compared to pure **Lov**. This suggests partial recrystallization, likely because the drug-loading capacity of the **PLA/Cs** matrix is exceeded, reducing its ability to stabilize **Lov** in an amorphous form. Similar recrystallization at high drug contents has been reported in polymer–drug systems due to in-droplet precipitation and excess crystal formation [24]. Furthermore, the **PCL55x** membranes exhibited melting temperatures (T_m) ranging from 140.8 °C to 145.7 °C, which is assigned as the melting point of **PLA**. This result is consistent with a previous study (the T_m of **PLA** is 140 °C) [25]. The T_m values of the composite membranes all shifted towards values greater than that of **PLA** and smaller than that of **Lov.** This shift reflects molecular interactions, particularly hydrogen bonding, between the OH group of **Lov** and the NH_2/OH groups of **Cs** or the ester groups of **PLA** [26]. These interactions not only stabilize the amorphous form but also suppress recrystallization during storage and release, thereby supporting long-term formulation stability.

In addition to these changes, two distinct endothermic signals appear in the DSC curves of the composites. The first corresponds to dehydration of

moisture bound to hydrophilic groups in **Cs**, while the second corresponds to the melting behavior of **Lov**. Notably, the melting point of **Lov** within the composites is substantially reduced compared to its pure crystalline state. This depression in melting temperature further confirms that **Lov** is predominantly present in a dispersed or amorphous state when incorporated into the **PLA/Cs** matrix.

Overall, the DSC results strongly align with the FESEM observations, both supporting the conclusion that at moderate loading levels, **Lov** is well-dispersed and stabilized in an amorphous form within the polymer network. At higher loadings, however, partial crystallization occurs, which could negatively impact dissolution performance and lead to burst-release effects.

3.4. Lov Release from the PCL55x Composites

The release behavior of **Lov** from **PCL55x** composites films was evaluated in buffer solutions at pH 2.0 and pH 7.4, simulating gastric and intestinal environments, respectively, at 37 °C. Both the medium's pH and the drug loading within the polymer matrix were found to significantly influence the release process.

The overall release profile of **Lov** displays two distinct phases: (i) an initial burst release, attributed mainly to **Lov** adsorbed on or near the film surface; and (ii) a subsequent sustained release phase, characterized by a gradual decrease in release rate. The latter is governed by diffusion through the **PLA/Cs** matrix and by swelling and partial hydrolysis of **PLA** under aqueous conditions [27]. In addition, interactions between functional groups of **Cs** and **Lov** with H^+ or OH^- in the medium contribute to the controlled release. Dipole interactions with water molecules, combined with matrix swelling and hydrolysis, promote gradual erosion of the polymer network. As a result, **Cs** and **Lov** are released as small aggregates, followed by the slow liberation of **Lov** molecules into solution, supporting a controlled and prolonged release pattern. The detailed release curves are presented in Fig. 6.

The effect of drug loading was systematically investigated in composites containing 5 – 20 wt.% **Lov** relative to the polymer matrix. In both acidic and neutral media, higher drug loadings led to faster release rates and larger cumulative amounts of **Lov** released. Among the tested formulations, the **PCL5510** sample exhibited the most favorable release profile: it showed slow and stable release in the acidic gastric environment (pH 2.0) and a markedly faster release under intestinal conditions (pH 7.4). This biphasic behavior is particularly advantageous, as it minimizes premature drug loss in the stomach while enhancing bioavailability upon intestinal absorption. These findings highlight **PCL5510** as a promising candidate for oral delivery of Lov. At higher drug contents (e.g., **PCL5515** and **PCL5520**), incomplete amorphization and partial crystallization of **Lov** (as evidenced by DSC and FESEM results) likely contributed to less uniform release, including sporadic burst effects. In contrast, the balanced drug loading of **PCL5510** ensured better molecular dispersion and more predictable release kinetics.

Notably, the release mechanism observed here contrasts with many existing carrier systems. Solid lipid nanoparticles (SLNs) and polymer nanoparticles (e.g., PLGA, PEG-PLA) often exhibit pronounced burst release within the first 2 – 4 hours, limiting dose control and increasing side-effect risk [28]. Likewise, alginate- or gelatin-based hydrogels, though capable of sustained release, tend to degrade rapidly under acidic conditions, resulting in uncontrolled release profiles [18]. In comparison, the **PLA/Cs/Lov** composite films not only maintained controlled release but also responded selectively to environmental pH, providing targeted delivery at specific gastrointestinal sites.

Overall, the **PLA/Cs/Lov** system, particularly the **PCL5510** formulation, demonstrates a synergistic balance between stability, pH sensitivity, and controlled release, offering significant promise for the oral delivery of poorly soluble statins such as **Lov**.

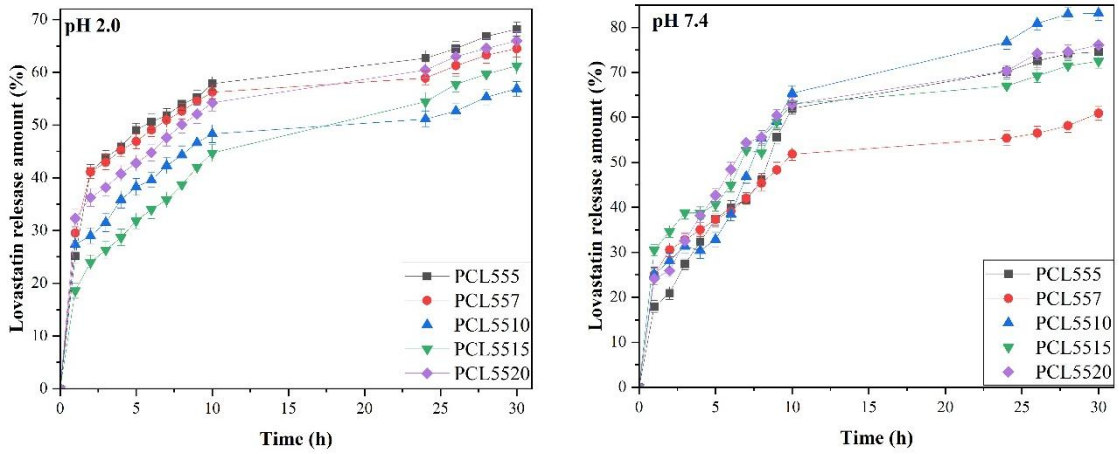

Fig. 6. Lov release profile from the **PCL55x** at pH 2.0 and pH 7.4

4. Conclusion

This study successfully fabricated **PLA/Cs/Lov** composite films and confirmed stable hydrogen bonding interactions among the components. DSC analysis indicated the conversion of Lov from its crystalline state (T_m) 174.6 ^oC to an amorphous state or molecular dispersion in moderately loaded samples (**PCL555, PCL557, PCL5510**). These interactions stabilize the amorphous form and suppress recrystallization. FESEM images confirmed the morphological transition into smaller spherical particles, with the **PCL5510** sample (10 wt.% Lov) achieving optimal dispersion, characterized by uniform particles sized approximately $0.2 - 0.5$ μm. In terms of release, **PCL5510** exhibited an ideal biphasic profile, demonstrating slow and stable release in the gastric environment (pH 2.0) and markedly faster release in the intestinal environment (pH 7.4). These findings confirm the **PCL5510** formulation as a promising candidate for controlled oral delivery of Lovastatin, balancing stability, pH sensitivity, and controlled release kinetics. These findings suggest a direction for developing biological drug-carrying material systems with dual functions: serving as both a biological scaffold and a drug delivery system. However, further in-depth studies on drug release kinetics, biocompatibility, and *in vivo* pharmacological efficacy are necessary to confirm the clinical application potential of this composite film system.

References

[1] S. Istvan and J. Deisenhofer, Structural mechanism for statin inhibition of HMG-CoA reductase, Science, vol. 292, no. 5519, pp. 1160–1164, May 2001. https://doi.org/10.1126/science.1059344

[2] Endo A., The discovery and development of HMG-CoA reductase inhibitors, Journal of Lipid Research, vol. 33, iss. 11, pp. 1569–1582, Nov. 1992. https://doi.org/10.1016/S0022-2275(20)41379-3

[3] Kazi M., Al-Swairi M., Ahmad A., Raish M., Alanazi F. K., Badran M. M., Khan A. A., Alanazi A. M. and Hussain M. D., Evaluation of self-nanoemulsifying drug delivery systems (SNEDDS) for poorly water-soluble talinolol: preparation, in vitro and in vivo assessment, Frontiers in Pharmacology, vol. 10, May 2019, Art. no. 459. https://doi.org/10.3389/fphar.2019.00459

[4] Liu D., Yang F., Xiong F. and Gu N., The smart drug delivery system and its clinical potential, Theranostics, vol. 6, no. 9, pp. 1306–1323, 2016. https://doi.org/10.7150/thno.14858

[5] Rautio J., Meanwell N. A., Di L., and Hageman M. J., The expanding role of prodrugs in contemporary drug design and development, Nature Reviews Drug Discovery, vol. 17, no. 8, pp. 559–587, Apr. 2018. https://doi.org/10.1038/nrd.2018.46

[6] Middleton J. C. and Tipton A. J., Synthetic biodegradable polymers as orthopedic devices, Biomaterials, vol. 21, iss. 23, pp. 2335–2346, Dec. 2000. https://doi.org/10.1016/S0142-9612(00)00101-0

[7] Mawazi S. M., Kumar M., Ahmad N., Ge Y., and Mahmood S., Recent applications of chitosan and its derivatives in antibacterial, anticancer, wound healing, and tissue engineering fields, Polymers, vol. 16, iss. 10, May 2024, Art. no. 1351. https://doi.org/10.3390/polym16101351

[8] Dash M., Chiellini F., Ottenbrite R. M., and Chiellini E., Chitosan - a versatile semi-synthetic polymer in biomedical applications, Progress in Polymer Science, vol. 36, iss. 8, pp. 981–1014, Aug. 2011. https://doi.org/10.1016/j.progpolymsci.2011.02.001

[9] Moldovan A., Cuc S., Prodan D., Rusu M., Popa D., Taut A. C., Petean I., Bomboş D., Doukeh R., and Nemes O., Development and characterization of polylactic acid (PLA)-based nanocomposites used for food packaging, Polymers, vol. 15, iss. 13, Jun. 2023, Art. no. 2855. https://doi.org/10.3390/polym15132855

[10] Dimzon I. K. D. and Knepper T. P., Degree of deacetylation of chitosan by infrared spectroscopy and partial least squares, International Journal of Biological Macromolecules, vol. 72, no. 1, pp. 939–945, Jan. 2015. https://doi.org/10.1016/j.ijbiomac.2014.09.050

[11] El-Araby A., Janati W., Ullah R., Ercisli S., and Errachidi F., Chitosan, chitosan derivatives, and chitosan-based nanocomposites: eco-friendly materials for advanced applications (a review), Frontier in Chemistry, vol. 11, Jan. 2024, Art. no. 1327426. https://doi.org/10.1089/fchem.2023.1327426

[12] Nguyen L. N., Vu M. Q., La G. C., Nguyen C. T., Hoang D. T., Tran D. T. T., Thai H., and Vu T. Q., Assessment of hemostatic ability of biomaterial based on chitosan and Eclipta prostrata L. extract, Biomedical Materials, vol. 19, 2024, Art. no. 035026. https://doi.org/10.1088/1748-605X/ad386e

[13] Pallipurath A. R., Skelton J. M., Britton A., Willneff E. A., and Schroeder S. L. M., Bulk and surface conformations in solid-state lovastatin: spectroscopic and molecular dynamics studies, Crystals, vol. 11, no. 5, May 2021, Art. no. 509. https://doi.org/10.3390/cryst11050509

[14] Vu T. T. T., Nguyen N. T. H., Vu M. Q., Nguyen L. N., Nguyen V. T. B., and Vu T. Q., Synthesis and characterization of chitosan/carrageenan/polyaniline-based biocomposite as lovastatin carrier and its drug release ability in buffer solutions, HNUE Journal of Science, vol. 68, iss. 3, pp. 46–74, 2023. https://doi.org/10.18173/2354-1059.2023-0061

[15] GhavamiNejad A., Ashammakhi N., Wu X. Y., and Khademhosseini A., Crosslinking strategies for 3D bioprinting of polymeric hydrogels, Small, vol. 16, iss. 35, Jul. 2020, Art. no. 2002931. https://doi.org/10.1002/smll.202002931

[16] Hatcher L. E., Li W., Payne P., Benyahia B., Rielly C. D., and Wilson C. C., Tuning morphology in active pharmaceutical ingredients: controlling the crystal habit of lovastatin through solvent choice and non-size-matched polymer additives, Crystal Growth & Design, vol. 20, iss. 9, pp. 5854–5862, Aug. 2020. https://doi.org/10.1021/acs.cgd.0c00470

[17] Ha H. M., Vu M. Q., Vu T. T. T., Dao T. T. P., Pham D. T., Nguyen V. T. B., Duong L. K., Nguyen L. N., Doan O. T. Y., Nguyen C. T., Thai H., and Vu T. Q., Evaluation of the effect of the chitosan/carrageenan ratio on lovastatin release from chitosan/carrageenan based biomaterials, Vietnam Journal of Chemistry, vol. 60, iss. 1, pp. 72–78, Oct. 2022. https://doi.org/10.1002/vjch.202200078

[18] Thai H., Nguyen C. T., Thach L. T., Tran M. T., Huynh D. M., Nguyen T. T. T., Le G. D., Can M. V., Tran L. D., Bach G. L., Kavitha Ramadass, C. I. Sathish, and Quan Van Le, Characterization of chitosan/alginate/lovastatin nanoparticles and investigation of their toxic effects in vitro and in vivo, Scientific Reports, vol. 10, no. 1, pp. 909, Jan. 2020. https://doi.org/10.1038/s41598-020-57666-8

[19] Shen M., Zheng L., Koole L. H., Polymeric microspheres designed to carry crystalline drugs at their surface or inside cavities and dimples, Pharmaceutics, vol. 15, iss. 8, 2023, Art. no. 2146. https://doi.org/10.3390/pharmaceutics15082146

[20] Sun Y. and Long D., Preparation, characterization and in vitro/in vivo evaluation of lovastatin-loaded PLGA microspheres by local administration for femoral head necrosis, Drug Design, Development and Therapy, vol. 15, pp. 601–610, Feb. 2021. https://doi.org/10.2147/DDDT.S286306

[21] Bhujbal S. V., Mitra B., Jain U., Gong Y., Agrawal A., Karki S., Taylor L. S., Kumar S., and Zhou Q. Pharmaceutical amorphous solid dispersion: a review of manufacturing strategies, Acta Pharmaceutica Sinica B, vol. 11, iss. 8, pp. 2505–2536, Aug. 2021. https://doi.org/10.1016/j.apsb.2021.05.014

[22] Patel R. P. and Mayur M. P., Physicochemical characterization and dissolution study of solid dispersions of lovastatin with polyethylene glycol 4000 and polyvinylpyrrolidone K30, Pharmaceutical Development and Technology, vol. 12, iss. 1, pp. 21–33, Oct. 2008. https://doi.org/10.1080/10837450601166510

[23] Nguyen C. T., Thach L. T., Le G. D., Ngo T. P.,Vu H. T., and Thai Hoang, Effect of polycaprolactone on characteristics and morphology of alginate/chitosan/lovastatine composite films, Vietnam Journal of Science and Technology, vol. 56, iss. 4A, pp. 13–21, 2018. https://doi.org/10.15625/2525-2518/56/4A/12738

[24] Li W., Chen J., Zhao S., Huang T., Ying H., Trujillo C., Molinaro G., Zhou Z., Jiang T., Liu W., Li L., Bai Y., Quan P., Ding Y., Hirvonen J., Yin G., Santos H., Fan J., and Liu D., High drug-loaded microspheres enabled by controlled in-droplet precipitation promote functional recovery after spinal cord injury, Nature Communications, vol. 13, no. 1, Mar. 2022, Art. no. 1262. https://doi.org/10.1038/s41467-022-28787-7

[25] Pantani R., Volpe V., Titomanlio G., Foam injection molding of poly(lactic acid) with environmentally friendly physical blowing agents, Journal of Materials Processing Technology, vol. 214, no. 12, pp. 3098–3107, 2014. https://doi.org/10.1016/j.jmatprotec.2014.07.002

[26] Vlachopoulos A., Karlioti G., Balla E., Daniilidis V., Kalamas T., Stefanidou M., Bikiaris N. D., Christodoulou E., Koumentakou I., and Karavas E., and Bikiaris D. N., Poly(lactic acid)-based microparticles for drug delivery applications: an overview of recent advances, Pharmaceutics, vol. 14, iss. 2, Feb. 2022, Art. no. 359. https://doi.org/10.3390/pharmaceutics14020359

[27] Liu C., Zhang D., Li D., Jiang D., and Chen X., Preparation and characterization of biodegradable polylactide (PLA) microspheres encapsulating ginsenoside Rg3, Chemistry Research in Chinese Universities, vol. 24, no.5, pp. 588–591, Sep. 2008. https://doi.org/10.1016/S1005-9040(08)60124-5

[28] Pandey S., Shaikh F., Gupta A., Tripathi P., and Yadav J. S., A recent update: solid lipid nanoparticles for effective drug delivery, Advanced Pharmaceutical Bulletin, vol. 12, iss. 1, 2002, Art. no. 7. https://doi.org/10.34172/apb.2022.007